

START

9513334.0019

0039637

16

PNL-10163
UC-2030

FERROCYANIDE TANK SAFETY PROJECT

COMPUTATIONAL ANALYSIS OF COUPLED
FLUID, HEAT, AND MASS TRANSPORT IN
FERROCYANIDE SINGLE-SHELL TANKS:
FY 1994 INTERIM REPORT

B. P. McGrail

November 1994

Prepared for
the U.S. Department of Energy
under Contract DE-AC06-76RLO 1830

Pacific Northwest Laboratory
Richland, Washington 99352



DISCLAIMER

This report was prepared as an account of work sponsored by an agency of the United States Government. Neither the United States Government nor any agency thereof, nor Battelle Memorial Institute, nor any of their employees, makes any warranty, expressed or implied, or assumes any legal liability or responsibility for the accuracy, completeness, or usefulness of any information, apparatus, product, or process disclosed, or represents that its use would not infringe privately owned rights. Reference herein to any specific commercial product, process, or service by trade name, trademark, manufacturer, or otherwise does not necessarily constitute or imply its endorsement, recommendation, or favoring by the United States Government or any agency thereof, or Battelle Memorial Institute. The views and opinions of authors expressed herein do not necessarily state or reflect those of the United States Government or any agency thereof.

PACIFIC NORTHWEST LABORATORY
operated by
BATTELLE MEMORIAL INSTITUTE
for the
UNITED STATES DEPARTMENT OF ENERGY
under Contract DE-AC06-76RLO 1830

Printed in the United States of America

Available to DOE and DOE contractors from the
Office of Scientific and Technical Information, P.O. Box 62, Oak Ridge, TN 37831;
prices available from (615) 576-8401. FTS 626-8401.

Available to the public from the National Technical Information Service,
U.S. Department of Commerce, 5285 Port Royal Rd., Springfield, VA 22161.

SUMMARY

A computer modeling study was conducted to determine whether natural convection processes in single-shell tanks containing ferrocyanide wastes could generate localized precipitation zones that significantly concentrate the major heat-generating radionuclide, ^{137}Cs . A computer code was developed that simulates coupled fluid, heat, and single-species mass transport on a regular, orthogonal finite-difference grid. The analysis showed that development of a "hot spot" is critically dependent on the temperature dependence for the solubility of $\text{Cs}_2\text{NiFe}(\text{CN})_6$ or $\text{CsNaNiFe}(\text{CN})_6$. For the normal case, where solubility increases with increasing temperature, the net effect of fluid flow, heat, and mass transport is to disperse any local zones of high heat generation rate. As a result, hot spots cannot physically develop for this case. However, assuming a retrograde solubility dependence, the simulations indicate the formation of localized deposition zones that concentrate the ^{137}Cs near the bottom center of the tank where the temperatures are highest. Recent experimental studies suggest that $\text{Cs}_2\text{NiFe}(\text{CN})_6(\text{c})$ does not exhibit retrograde solubility over the temperature range 25°C to 90°C and NaOH concentrations to 5 M . Assuming these preliminary results are confirmed, no natural mass transport process exists for generating a hot spot in the ferrocyanide single-shell tanks.

NOMENCLATURE

a_i	stoichiometric coefficient
b	Forcheimer constant
c	species concentration (mol/m ³)
C_v	heat capacity (J/g·°C)
D	diffusion coefficient (m ² /s)
g	gravitational constant (m/s ²)
G	decay heat generation rate (J/mol)
ΔH	enthalpy (J/mol)
k	permeability (m ²)
K_s^o	equilibrium constant at T_o
K_s	equilibrium constant at T
P	fluid pressure (Pa)
\dot{q}	heat generation rate (J/m ³ ·s)
R	gas constant (J/mol·K)
t	time (s)
T	temperature
T_o	reference temperature
\mathbf{V}	fluid velocity vector (m/s)
v_x, v_y	fluid velocity vector components (m/s)
w	width of tank (m)
h	height of sludge in tank (m)
α	thermal diffusivity (m ² /s)
β	dimensionless heat capacity ratio, $\epsilon(\rho C_v)_l / \overline{\rho C_v}$
ϵ	porosity
κ	thermal conductivity (J/m·s·°C)
ρ	density (g/m ³)
ν	kinematic viscosity (m ² /s)
μ	absolute viscosity (g/m·s)
λ	decay constant (s ⁻¹)

Subscripts

l = liquid, s = porous sludge

CONTENTS

SUMMARY.....	iii
NOMENCLATURE	v
INTRODUCTION	1
THEORY	3
MODEL DESCRIPTION	3
SOLUTION METHOD	4
Numerical Methods	5
RESULTS.....	7
FULLY COUPLED FLUID, HEAT, AND MASS TRANSPORT.....	7
Normal Temperature Dependence ($\Delta H < 0$).....	8
Retrograde Temperature Dependence ($\Delta H > 0$).....	9
DISCUSSION.....	9
REFERENCES	11

FIGURES

1	Schematic Illustration of Two-Dimensional Conceptualization of Waste Tank	3
2	Base Case Centerline Temperature Profiles for a Hypothetical Waste Tank	7
3	Typical Bifurcated Flow Field in Porous Waste Sludge.....	8
4	Temperature Contour Map at $t=14$ y	8
5	Concentration Contour Map of ^{137}Cs at 6 y (a) and 14 y (b).....	8
6	Temperature and ^{137}Cs Contour Map at $t=25$ y Assuming Retrograde Solubility for $\text{Cs}_2\text{NiFe}(\text{CN})_6$	9
A.1	Example Finite-Difference Grid for Solution of Coupled Equation System.....	A-1

INTRODUCTION

Beginning in the early 1940s, radioactive wastes were generated on the Hanford Site in Washington state from processing irradiated uranium fuels to extract plutonium for the U.S. nuclear weapons program. The wastes are primarily stored underground, as alkaline slurries in 500,000- to 1,000,000 gallon capacity steel tanks. Through 1964, 149 of the tanks were built with a single-shell design (SST) consisting of a concrete shell and steel liner. In 1971, the design was changed to a double-shell (DST) configuration consisting of a primary and secondary steel tank surrounded by a concrete shell. To date, the total volume of waste in storage is more than 40,000,000 gal.¹

During the 1950s, Hanford Site scientists developed a carrier precipitation process to remove radioactive cesium from tank waste liquids. By removing this heat-generating radionuclide from the waste stream, it was possible to discharge the treated liquids to the ground, and thus obtain additional tank storage space without constructing more tanks. The process used salts of either sodium [$\text{Na}_4\text{Fe}(\text{CN})_6 \cdot 10\text{H}_2\text{O}$] or potassium [$\text{K}_4\text{Fe}(\text{CN})_6 \cdot 3\text{H}_2\text{O}$] ferrocyanide to precipitate the cesium, ideally as $\text{Cs}_2\text{NiFe}(\text{CN})_6$ or $\text{CsNaNiFe}(\text{CN})_6$. In practice, the compound(s) precipitated in the process are not completely known. Overall, 140 metric tons of ferrocyanides were added to the SSTs.

In 1990, safety concerns about the SSTs containing ferrocyanides were raised.² The safety of these tanks is at issue because ferrocyanide, in the presence of an oxidizer such as NaNO_3 or NaNO_2 , is explosively combustible when sufficiently concentrated and exposed to elevated temperatures.^{3,4} The SSTs contain abundant amounts of nitrate and nitrite⁵ with molar ratios ranging from 30:1 to 50:1 mol NO_3 :mol $\text{Fe}(\text{CN})_6$. Consequently, SSTs containing ferrocyanide wastes currently exist in a stable but theoretically combustible state.

Laboratory investigations of the energetics of ferrocyanide reactions with nitrate and nitrite salts show that runaway exotherms do not occur below temperatures of at least 220° to 250°C. Although temperatures are measured at only one radial location in the SSTs, maximum temperatures are less than 55°C, far below the required ignition temperature. Barring development of a thermally isolated zone or "hot spot", the ferrocyanide wastes are safe from a propagating exothermic reaction under these conditions.

Heat conduction studies of SSTs have been conducted by Grigsby et al.⁵ using the HEATING7 code⁶ to analyze slabs of varying thickness with various volumetric heating rates. They found, for a slab with an edge length equal in diameter to the tank, that the available heat generation rate could only raise the slab temperature to 90°C, far below temperatures needed to sustain a propagating exothermic reaction. However, using spherical geometry with a radius for the hot spot of 1.2 m, a center temperature of 200°C could be reached by concentrating the decay heat by factors of 75 to 500 over the average. Similar results were found by Dickinson et al.⁷ although lower concentration factors were shown to be needed (≈ 20) for a zone in the shape of a square cylinder of 5 m height and diameter. Although no supporting results were given, the authors conclude that no credible mechanism exists for concentrating the tank heat load by these large factors.

Unfortunately, the heat conduction models used in the simulations described above are incapable of modeling radionuclide mass transport as a process for redistribution of the tank heat load. Mass transport processes could potentially concentrate the heat generating radionuclides in local zones because of thermal or chemical potential gradients. For example, mineral deposition reactions play a key role in the development of geothermal ore deposits.^{8,9}

In a previous report, results from the first modeling studies of coupled heat and mass transport in ferrocyanide SSTs were presented.¹⁰ A constant fluid velocity was assumed as derived from a fluid stability analysis or taken from calculations done with the TEMPEST code.¹¹ In this work, our previous studies are extended to include simultaneous fluid, heat, and mass transport processes. The purpose is to determine under what conditions mass redistribution of ^{137}Cs may occur and to assess whether coupling fluid flow in the model has any significance to the development of "hot spots" in ferrocyanide waste tanks.

THEORY

The fundamental processes of interest in this study include

- heat transfer and internal heat generation from radioactive decay
- mass transport
- fluid flow.

In constructing a model to analyze these processes, an idealized view of a SST containing ferrocyanide-bearing waste sludges was used as illustrated schematically in Figure 1. The tank is idealized in two-dimensions, and the sludge is represented as a fluid-saturated porous medium. Relatively rapid air circulation is assumed to maintain a constant temperature in the tank headspace.

Recent studies by Epstein et al.¹² indicate that ferrocyanide sludges do not exhibit porous medium rheological properties. However, in their experiments, the ferrocyanide sludges are exposed to high thermal power densities. This raised the pore water temperature above boiling so that water vapor bubbles formed in the sludge in a matter of a few minutes. The force exerted on the sludge particles as the bubbles formed was more than sufficient to overcome the yield stress and induce bulk flow of the sludge.

As will be shown later in this report, the maximum calculated fluid velocities in the sludge using a porous medium model are on the order of $\mu\text{m/s}$. The pressure

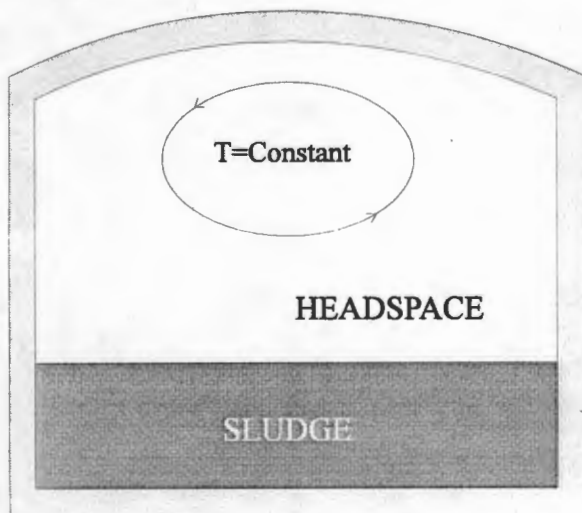


Figure 1. Schematic Illustration of Two-Dimensional Conceptualization of Waste Tank

gradient driving this "microconvection" is insufficient to perturb the sludge mechanically. It is further assumed here that no other process, such as radiolytic generation of gases, is occurring in the tank that could significantly perturb the sludge. Given these assumptions, the sludge may be reasonably treated as a static porous medium.

Essentially, the dryout studies of Epstein et al.¹² complement this study. Epstein et al. begin their theoretical analysis by assuming that a "hot spot" has formed in the sludge and proceed to analyze the behavior of the material from that point. A more fundamental question is posed in this study where we seek to understand how a "hot spot" could physically form as a result of natural fluid, heat, and mass transport processes.

MODEL DESCRIPTION

The model consists of the complete set of continuity, momentum, energy, single-species transport, mass-action, and mass-balance equations. These are:

1) Continuity

$$\nabla \cdot \mathbf{V} = 0 \quad (1)$$

2) Momentum

$$\rho \nabla^2 \mathbf{V} - \frac{\rho}{k} \mathbf{V} - \frac{b}{k} |\mathbf{V}| \mathbf{V} = \frac{1}{\rho} \nabla P - \mathbf{g} \quad (2)$$

3) Energy

$$\frac{\partial T}{\partial t} = \nabla \cdot (\bar{\kappa} \nabla T) - \epsilon (\rho C_v)_l \mathbf{V} \cdot \nabla T + \dot{q} \quad (3)$$

4) Transport

$$\frac{\partial c_l}{\partial t} = \nabla \cdot (D \nabla c_l) - \mathbf{V} \cdot \nabla c_l - \lambda c_l \quad (4)$$

5) Mass-Action

$$c_l = \left\{ \begin{array}{l} \left(\frac{K_s(T)}{\prod_{j=1}^N c_j^{a_j}} \right)^{a_l}, \quad c_s > 0 \\ c_l, \quad c_s = 0 \end{array} \right\} \quad (5)$$

6) Mass-Balance

$$\frac{\partial c_s}{\partial t} = -\left(\varepsilon \frac{\partial c_l}{\partial t} + \lambda c_s\right) \quad (6)$$

$$\text{where } \overline{\rho C_v} = \varepsilon(\rho C_v)_l + (1-\varepsilon)(\rho C_v)_s \quad (7)$$

$$\overline{\kappa} = \varepsilon \kappa_l + (1-\varepsilon)\kappa_s \quad (8)$$

$$K_s(T) = K_s^0 - \frac{\Delta H}{R} \left(\frac{1}{T_0} - \frac{1}{T} \right) \quad (9)$$

The solution to the momentum equation can be simplified by examining the orders of magnitude for each term on the left-hand side of Equation (2), given expected values for properties of the sludges in the ferrocyanide tanks. Assuming $\mu=O(1)$, $k=O(10^{-13})$, $b=O(10^{-8})$, and $V=O(10^{-6})$, the orders of magnitude for the first second and third terms on the left-hand side of Equation (2) are $O(10^{-6})$, $O(10^7)$, $O(10^{-7})$, respectively. Obviously, the second term dominates by many orders of magnitude so the momentum equation can be reduced to the well-known Darcy equation

$$\frac{v}{k} \mathbf{V} = -\frac{1}{\rho} \nabla P + \mathbf{g} \quad (10)$$

The equation system (1), (3)-(6), and (10) is the equation system where a solution is sought. An overview of the solution methods used is given in the next section.

SOLUTION METHOD

In a 2-D cartesian coordinate system, Equations (3) and (4) become

$$\frac{\partial T}{\partial t} = \overline{\alpha}(T) \left(\frac{\partial^2 T}{\partial x^2} + \frac{\partial^2 T}{\partial y^2} \right) - \beta(T) \left(v_x \frac{\partial T}{\partial x} + v_y \frac{\partial T}{\partial y} \right) + Q(x, y, t), \quad 0 < x < w, 0 < y < h, t > 0 \quad (11)$$

$$\frac{\partial c_l}{\partial t} = D \left(\frac{\partial^2 c_l}{\partial x^2} + \frac{\partial^2 c_l}{\partial y^2} \right) - v_x \frac{\partial c_l}{\partial x} - v_y \frac{\partial c_l}{\partial y} - \lambda c_l, \quad 0 < x < w, 0 < y < h, t > 0 \quad (12)$$

where

$$\overline{\alpha}(T) = \frac{\overline{\kappa}}{\rho C_v}, \quad \beta(T) = \frac{\varepsilon(\rho C_v)_l}{\rho C_v} \quad (13)$$

In Equation (12), it is assumed that the species diffusion coefficient is constant and independent of

both temperature and c_l . The energy (11) and solute transport equation (12) are coupled through the heat generation rate term $Q(x, y, t)$ which is given by

$$Q(x, y, t) = \frac{[c_s(x, y, t) + c_l(x, y, t)]G}{\rho C_v} \quad (14)$$

where G = decay heat generation rate, J/mol.

Equation (11) is solved subject to the following initial and boundary conditions:

$$T(x, y, 0) = T_0(x, y), \quad 0 \leq x \leq w, 0 \leq y \leq h \quad (15)$$

$$\left\{ \begin{array}{l} T(0, y, t) = T_1 \\ \overline{\alpha} \frac{\partial T}{\partial x} \Big|_{x=0} = F_1 \end{array} \right\} \left\{ \begin{array}{l} T(w, y, t) = T_3 \\ \overline{\alpha} \frac{\partial T}{\partial x} \Big|_{x=w} = F_3 \end{array} \right\}, \quad 0 \leq y \leq h, t > 0 \quad (16)$$

$$\left\{ \begin{array}{l} T(x, 0, t) = T_2 \\ \overline{\alpha} \frac{\partial T}{\partial y} \Big|_{y=0} = F_2 \end{array} \right\} \left\{ \begin{array}{l} T(x, h, t) = T_4 \\ \overline{\alpha} \frac{\partial T}{\partial y} \Big|_{y=h} = F_4 \end{array} \right\}, \quad 0 < x < w, t > 0 \quad (17)$$

where T_1, T_2, T_3, T_4 are specified wall temperatures (Dirichlet boundary) and F_1, F_2, F_3, F_4 are specified heat fluxes at each wall (Neumann boundary). Equation (15) specifies that the initial temperature is a known function of x and y . Equation (16) specifies that the vertical walls are held at either a constant temperature or constant thermal flux as does Equation (17) for the bottom wall and surface of the waste sludge. Of course, an adiabatic wall is simply a special case where $F=0$.

For the solute transport equation (12), the initial and boundary conditions are

$$c_l(x, y, 0) = c_0(x, y), \quad 0 \leq x \leq w, 0 \leq y \leq h \quad (18)$$

$$\frac{\partial c_l}{\partial x} \Big|_{x=0, x=w} = 0, \quad 0 \leq y \leq h, t > 0 \quad (19)$$

$$\frac{\partial c_l}{\partial y} \Big|_{y=0, y=h} = 0, \quad 0 < x < w, t > 0. \quad (20)$$

Equation (18) specifies that the initial concentration is a known function of x and y . Equations (19) and (20) specify that the tank walls are impermeable.

The continuity and fluid momentum equations are

$$\frac{\partial v_x}{\partial x} + \frac{\partial v_y}{\partial y} = 0, \quad 0 \leq x \leq w, 0 \leq y \leq h \quad (21)$$

$$\frac{\nu}{k} v_x = -\frac{1}{\rho} \frac{\partial p}{\partial x} \quad (22)$$

$$\frac{\nu}{k} v_y = -\frac{1}{\rho} \frac{\partial p}{\partial y} - g \quad (23)$$

The pressure variable is eliminated by taking $\partial/\partial y$ and $\partial/\partial x$ of Equations (22) and (23), respectively, and invoking the Boussinesq approximation¹³ to give

$$\frac{\mu}{k} \left(\frac{\partial v_y}{\partial x} - \frac{\partial v_x}{\partial y} \right) = -g \frac{\partial \rho}{\partial x} \quad (24)$$

Next, a vorticity function is defined as

$$\omega(x, y) = \frac{\partial v_y}{\partial x} - \frac{\partial v_x}{\partial y} \quad (25)$$

so Equation (24) becomes

$$\frac{\mu}{k} \omega(x, y) = -g \frac{\partial \rho}{\partial x} \quad (26)$$

We now define a stream function

$$v_x = \frac{\partial \Psi}{\partial y}, \quad v_y = -\frac{\partial \Psi}{\partial x} \quad (27)$$

which is easily shown to satisfy the continuity equation (21). Substituting Equation (27) into (25) gives

$$\nabla^2 \Psi(x, y) = -\omega(x, y). \quad (28)$$

Combining Equations (26) and (28), we arrive at the final expression

$$\nabla^2 \Psi(x, y) = \frac{kg}{\mu} \frac{\partial \rho}{\partial x}. \quad (29)$$

The solution to this elliptical equation defines the fluid velocity field through use of the identities (27). The boundary conditions are

$$\left. \frac{\partial \Psi}{\partial x} \right|_{y=0, y=h} = 0, \quad 0 \leq x \leq w \quad (30)$$

$$\left. \frac{\partial \Psi}{\partial y} \right|_{x=0, x=w} = 0, \quad 0 \leq y \leq h \quad (31)$$

which simply specifies that the y -component of the fluid velocity is zero along the top and bottom walls and the x -component of the fluid velocity is zero along the vertical walls.

Numerical Methods

The numerical solution of Equations (5-6), (11-12), and (29) was performed using the method of finite-differences on a regular 2-D orthogonal grid. For the advection-diffusion type equations (11-12), the diffusive terms were treated with the classic Crank-Nicolson scheme¹⁴ and the advective terms treated with Roe's Superbee total variation diminishing (TVD) method.¹⁵ The TVD method helps minimize numerical dissipation of sharp fronts in advection dominated transport problems. The stream function equation (29) was solved with a successive over-relaxation scheme.¹⁶ Details on the differencing scheme and numerical methods used are given in the Appendix.

The sequence used to solve the equation system was 1) solve Equation (11) for the temperature field, 2) solve Equation (29) for the stream function $\Psi(x, y)$ and obtain the velocity field from Equation (27), 3) solve Equations (5), (6), and (12) to obtain the concentration field. Iteration between the solvers for the temperature and velocity fields was not required as the temperature field varied in time much more slowly than the velocity field. Likewise, iterations between the solver for the temperature field and transport equation solver were not required as the concentration field varied much more slowly than the temperature field. The ability to sequentially solve this equation system without requiring iterations made the problem tractable for solution on a workstation class computer.

A computer code Tank Waste Simulator was developed to implement the solution method. Tank Waste Simulator runs under the Microsoft Windows™ operating environment and it takes advantage of the graphical user interface to provide access to all file I/O and data input needed to run the code and to view computed results on-screen in either a tabular format or graphically in a 2-D, high-resolution color plot.

RESULTS

As a basis for comparison with the other simulations reported in this section, the calculated temperature profiles for a hypothetical waste tank of 23 m diameter containing waste 10 m deep are shown first where it is assumed that no fluid flow, or mass transfer occurs. Thus, the simulation consists of solving the energy equation (12) for the case of pure conduction with internal heat generation from radioactive decay. The fluid density and thermal conductivity were assumed to be temperature dependent in accordance with published values for distilled water, and the heat capacity of the $\text{Na}_2\text{NiFe}(\text{CN})_6$ waste is given by $0.245+0.000273T$ J/g $\cdot^\circ\text{C}$. All other parameters were held constant and are listed in Table 1. Heat load is assumed to derive exclusively from radioactive decay of ^{137}Cs with a half-life of 30.23 y and generating 0.00472 W/Ci. The ^{137}Cs is assumed, initially, to be uniformly distributed at a concentration of 2×10^{-5} mol/kg, which corresponds to a volumetric heating rate of 1.78 W/m^3 . Initial temperature in the tank is assumed to be a uniform 25°C and the tank headspace is assumed to be held at a constant 30°C with the other tank walls taken as adiabatic surfaces. The predicted time-dependent vertical temperature profile at the tank centerline using these conditions is given in Figure 2. Because of the assumed adiabatic surfaces for the tank walls, the temperature profile varies little in the radial direction.

Table 1. Constant Parameters Used in Tank Heat and Mass Transport Simulations

Parameter	Value
<u>Waste</u>	
Porosity	0.4
Diffusion coefficient	$1.5 \times 10^{-5} \text{ cm}^2/\text{s}$
Tortuosity	1.0
Density	1.6 g/cm^3
Thermal conductivity	$1.7 \text{ W/m}\cdot^\circ\text{C}$
Permeability	10^{-14} m^2
<u>Fluid</u>	
Heat capacity	$4.19 \text{ J/g}\cdot^\circ\text{C}$

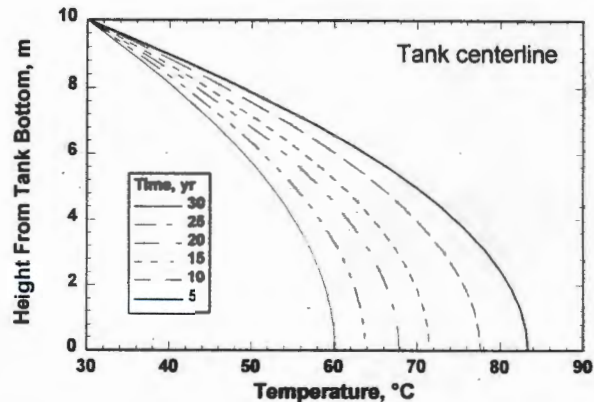


Figure 2. Base Case Centerline Temperature Profiles for a Hypothetical Waste Tank. Initial ^{137}Cs concentration = 2×10^{-5} mol/kg. No fluid flow or mass transport.

FULLY COUPLED FLUID, HEAT, AND MASS TRANSPORT

Several simulations were performed that fully couple fluid, heat, and mass transport processes. Because the temperature dependence for the density of the pore fluids in ferrocyanide waste sludges is unknown, the temperature dependence for the density of distilled water at 1 atm pressure was used as calculated by the empirical formula

$$\rho(T) = 0.49 + 4.37 \times 10^{-3} T - 1.14 \times 10^{-5} T^2 + 8.12 \times 10^{-8} T^3.$$

Permeability of the sludge was assumed to be constant and homogeneous at 10^{-14} m^2 . All other constant parameters are listed in Table 1.

Figure 3 illustrates a typical fluid velocity field generated with the Tank Waste Simulator code. The internal heat generated by radioactive decay establishes temperature gradients in the porous waste sludge, which generates a fluid density gradient. The density gradient generates an instability in the system that sets the fluid into motion. Along the colder outer walls of the tank, the more dense fluid sinks to the bottom of the tank whereas near the warmer center of the tank, the less dense fluid rises. The net result is the generation of a bifurcated velocity field as illustrated in Figure 3. Maximum fluid velocities occur at the tank centerline where the fluid is predicted to be rising vertically at

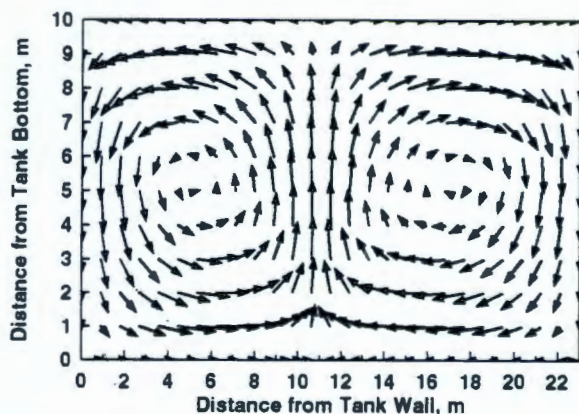


Figure 3. Typical Bifurcated Flow Field in Porous Waste Sludge

approximately 4×10^{-7} m/s or 13 m/y. In contrast, the fluid is nearly stagnant at the center of the vortices on both the left and right sides of the 2-D tank. In the following sections, the effects of heat and mass transport along these flow streamlines is illustrated.

Normal Temperature Dependence ($\Delta H < 0$)

Inspection of Equation (9) shows that for $T > T_0$, if $\Delta H < 0$, the solubility of $\text{Cs}_2\text{NiFe}(\text{CN})_6$ increases with increasing temperature and, if $\Delta H > 0$, the solubility decreases with increasing temperature. The phenomenon of decreasing solubility with increasing temperature is known as retrograde solubility. Examples of solids that exhibit this behavior in aqueous solution include CaCO_3 , LiF , and NaSO_4 . Simulations were run using a range of positive and negative values for ΔH .

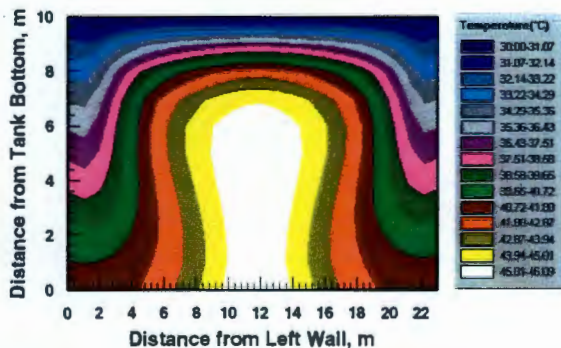


Figure 4. Temperature Contour Map at $t=14$ y. $\text{Log } K_s^0 = -19$; $\Delta H = -10$ kJ/mol.

Figure 4 shows the calculated temperature profile after 10 simulated years of fluid, heat, and mass transport in the waste sludge. A comparison with the centerline temperatures calculated for the case of no flow shows that circulation of the colder fluid from the top of tank reduces the peak centerline temperature by about 20°C .

Figures 5a and 5b show the calculated concentration profiles for ^{137}Cs at 6 and 14 y assuming a normal increasing solubility with temperature for $\text{Cs}_2\text{NiFe}(\text{CN})_6$ ($\Delta H = -10$ kJ/mol). At 6 years, diffusion and convection have established a deposition zone near the cooler top of the tank where the solubility is lowest. However, after 14 years, as shown in Figure 5b, the ^{137}Cs has dispersed nearly uniformly throughout the tank. The dispersion is caused by the convection of warm fluid from the bottom of the tank which dissolves the precipitate and then disperses the ^{137}Cs along the flow streamlines. Even though fluid velocities are small ($< 1 \mu\text{m/s}$), grid Peclet numbers ($v_p \Delta y / D$) are on the order of 100 near the center of the tank indicating that mass transport is dominated by convection over diffusion in these regions. Hence, it is not surprising to observe the ^{137}Cs migrating primarily along the flow streamlines as is clearly evident in Figure 5b.

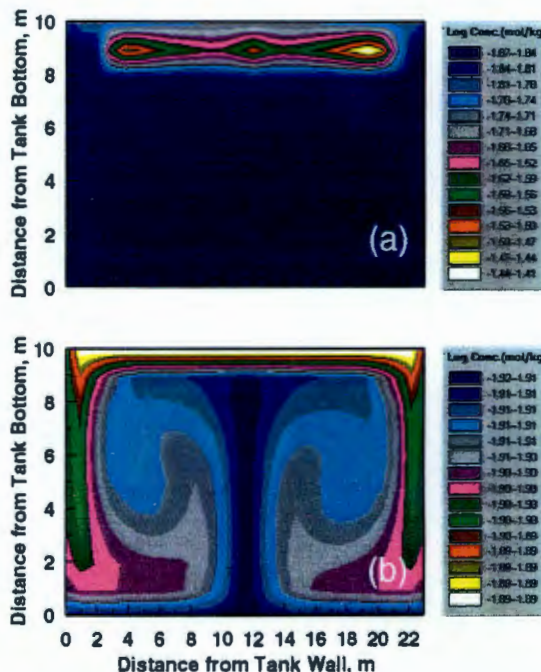


Figure 5. Concentration Contour Map of ^{137}Cs at 6 y (a) and 14 y (b). $\text{Log } K_s = -19$; $\Delta H = -10$ kJ/mol.

Retrograde Temperature Dependence ($\Delta H > 0$)

Figures 6a and 6b show the calculated temperature and ^{137}Cs concentration profiles after 25 y for the case where retrograde solubility for $\text{Cs}_2\text{NiFe}(\text{CN})_6$ was assumed ($\Delta H = 10 \text{ kJ/mol}$). In this case, the ^{137}Cs concentrates in zones near the bottom of the tank where the temperatures are highest. Maximum concentration factors of about 12 are predicted over the least concentrated portions of the tank. The redistribution of ^{137}Cs in these zones had little impact on the temperature profiles in the tank as sufficient convective mixing occurs to mitigate the increased heat generation rate.

DISCUSSION

The analysis of coupled fluid, heat, and mass transport processes in ferrocyanide SSTs indicates that the mechanism for development of a "hot spot" is dependent on the assumed temperature dependence for the solubility of $\text{Cs}_2\text{NiFe}(\text{CN})_6$. The net effect of coupled fluid flow, heat, and mass transport for the case where

$\Delta H < 0$ is dispersion of any local zone of high heat generation rate. As a result, hot spots cannot develop as a result of any conceivable natural diffusive or convective mass transfer process in the tank for this case.

However, our simulations indicate that localized concentration of heat-generating ^{137}Cs can occur if the $\text{Cs}_2\text{NiFe}(\text{CN})_6$ is retrograde soluble. The maximum concentration factors we observed were only about a factor of 12 over the least concentrated regions in the tank. However, this may be due to numerical dispersion inherent in the solution of the transport equation near steep concentration fronts. Numerical dispersion is particularly problematic in convection dominated regions as is the case near the tank centerline. Actual concentration factors could be higher. A check of the mass balance after the 25 year simulations indicated a mass loss of approximately 10% confirming that some numerical dispersion had occurred in the calculations. More advanced numerical algorithms are being investigated to better resolve the concentration fronts.

As long as water is present in the waste sludges, the simulations indicate that thermal buoyancy-driven convective heat transfer is sufficient to prevent development of a "hot spot." However, should water be removed from the tank either accidentally or purposely, the configuration of these zones is such that a "hot spot" could develop. The concentration factors indicated in our simulations are not of concern in terms of generating sufficient heat to raise the temperature of the "hot spot" to temperatures $>250^\circ\text{C}$, even in a dry-out scenario. However, given that the accuracy of these concentration factors is likely to be low, the modeling results cannot rule out the possibility of generating a "hot spot" of concern if the Cs-bearing ferrocyanide wastes have retrograde solubility.

Fortunately, experimental studies are under way to determine the temperature dependence for those compounds in the ferrocyanide tanks that contain the bulk of the precipitated heat generating radionuclides; that is ^{137}Cs and ^{90}Sr . Preliminary results indicate that the $\text{Cs}_2\text{NiFe}(\text{CN})_6(\text{c})$ has a normal temperature dependent solubility over the temperature range of 25° to 90°C and NaOH concentrations to 5 M. Assuming these preliminary results are confirmed, we conclude that no natural mass transport process exists for generating a hot spot in the ferrocyanide SSTs.

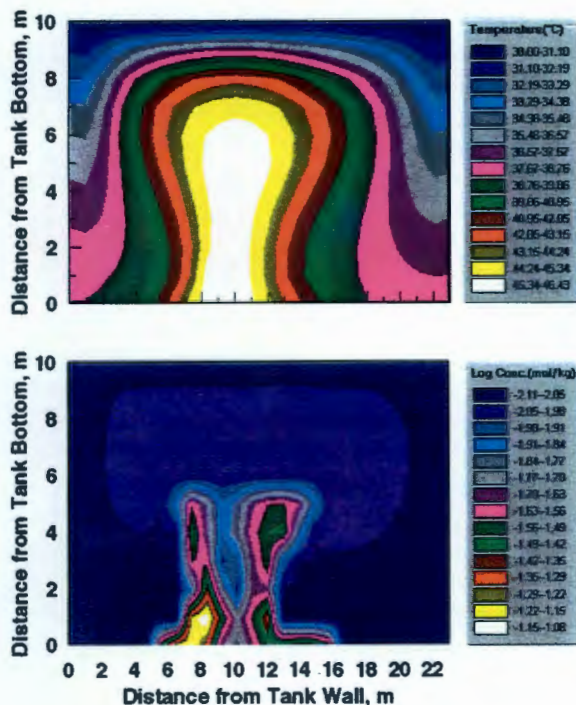


Figure 6. Temperature and ^{137}Cs Contour Map at $t = 25 \text{ y}$ Assuming Retrograde Solubility for $\text{Cs}_2\text{NiFe}(\text{CN})_6$. $\text{Log } K_s^0 = -19$; $\Delta H = 10 \text{ kJ/mol}$.

REFERENCES

- ¹Anderson, J. D. 1990. *A History of the 200 Area Tank Farms*. WHC-MR-0132, Westinghouse Hanford Company, Richland, Washington.
- ²Deaton, D. E. 1990. *Unreviewed Safety Question Regarding Tanks Containing Ferrocyanide*. Occurance Report, WHC-90-B003-R1, Update, 10-22-90, Westinghouse Hanford Company, Richland, Washington.
- ³Burger, L. L., and R. D. Scheele. 1988. *Interim Report: Cyanide Safety Issues*. PNL-7175, Pacific Northwest Laboratory, Richland, Washington.
- ⁴Burger, L. L., and R. D. Scheele. 1991. *The Reactivity of Cesium Nickel Ferrocyanide Towards Nitrate and Nitrite Salts*. PNL-7550, Pacific Northwest Laboratory, Richland, Washington.
- ⁵Grigsby, J. M., D. B. Bechtold, G. L. Borsheim, M. D. Crippen, D. R. Dickinson, G. L. Fox, D. W. Jeppson, M. Kummerer, J. M. McLaren, J. D. McCormack, A. Padilla, B. C. Simpson, and D. D. Stepnewski. 1992. *Ferrocyanide Waste Tank Hazard Assessment - Interim Report*. WHC-SD-WM-RPT-032, Rev. 1, Westinghouse Hanford Company, Richland, Washington.
- ⁶Childs, K. W. 1991. *HEATING 7.1 User's Manual*. K/CSD/TM-96, ORNL Martin Marietta, Oak Ridge, Tennessee.
- ⁷Dickinson, D. R., J. M. McLaren, G. L. Borsheim, and M. D. Crippen. 1993. *Credibility of Dryout in Ferrocyanide Sludge Due to Local Hot Spots*. WHC-EP-0648, Westinghouse Hanford Company, Richland, Washington.
- ⁸Sharp, J. M., and J. R. Kyle. 1988. *Hydrogeology*. Geologic Society of North America.
- ⁹Ellis, A. J., and W. A. J. Mahon. 1977. *Chemistry and Geothermal Systems*. Academic Press, New York.
- ¹⁰McGrail, B. P., D. S. Trent, G. Terrones, J. D. Hudson, and T. E. Michener. 1993. *Computational Analysis of Fluid Flow and Zonal Deposition in Ferrocyanide Single-Shell Tanks*. PNL-8876, Pacific Northwest Laboratory, Richland, Washington.
- ¹¹Trent, D. S., and L. L. Eyler. 1993. *TEMPEST-A Computer Program for Three-Dimensional, Time-Dependent Computational Fluid Dynamics: Theory Manual. Version T, Mod 3*. PNL-8857, Pacific Northwest Laboratory, Richland, Washington.
- ¹²Epstein, M., H. K. Fauske, M. D. Crippen, D. R. Dickinson, J. D. McCormack, R. J. Cash, J. E. Meacham, and C. S. Simmons. 1994. *Assessment of the Possibility of Ferrocyanide Sludge Dryout*. WHC-EP-0816, Westinghouse Hanford Company, Richland, Washington.
- ¹³Boussinesq, J. 1903. "Théorie Analytique de la Chaleur." *Gauthier-Villars* 2:172.
- ¹⁴Crank, J., and Nicholson. 1947. *Proc. Camb. Phil. Soc.* 43:50-67.
- ¹⁵Roe, P. L. 1985. "Some Contributions to the Modeling of Discontinuous Flows." *Lect. Appl. Math.* 22:163-193.
- ¹⁶Press, W. H., B. P. Flannery, S. A. Teukolsky, and W. T. Vetterling. 1986. *Numerical Recipes*. Cambridge University Press, United Kingdom.

9513334.0031

APPENDIX

FINITE DIFFERENCE EQUATIONS

APPENDIX FINITE DIFFERENCE EQUATIONS

Derived here are the finite-difference equations for solution of the heat and mass transport equations as described in the Theory section. The basic solution method is the alternating-direction implicit method originally developed by Peaceman and Rachford.¹ Explicitly developed here are the finite-difference equations for the energy equation (11). The difference equations for the diffusion-advection equation (12) are essentially the same with the exception of handling the mass action and mass balance constraints.

DERIVATION

Figure A.1 illustrates a typical domain of width w and height h with a finite-difference grid of m nodes in the x -direction and l nodes in the y -direction. First, the following notation is introduced for the spatial discretization variables. From second-order central difference formula

$$\begin{aligned}\delta_x^2 &= \Delta x^{-2}(T_{i-1,j} - 2T_{i,j} + T_{i+1,j}) \\ \delta_y^2 &= \Delta y^{-2}(T_{i,j-1} - 2T_{i,j} + T_{i,j+1})\end{aligned}\quad (\text{A1})$$

where Δx and Δy are the spatial step sizes. Using first-order upwind differencing, δ_x and δ_y are given by

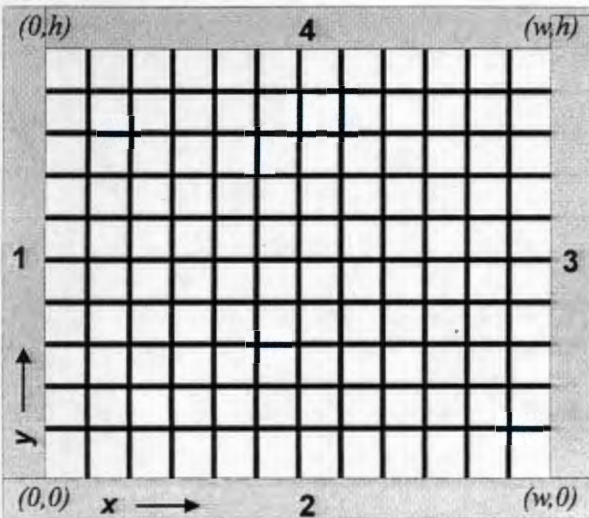


Figure A.1. Example Finite-Difference Grid for Solution of Coupled Equation System

$$\delta_x = \begin{cases} \frac{(T_{i,j} - T_{i-1,j})}{\Delta x}, & v_x > 0 \\ \frac{(T_{i+1,j} - T_{i,j})}{\Delta x}, & v_x < 0 \end{cases} \quad (\text{A2})$$

$$\delta_y = \begin{cases} \frac{(T_{i,j} - T_{i,j-1})}{\Delta y}, & v_y > 0 \\ \frac{(T_{i,j+1} - T_{i,j})}{\Delta y}, & v_y < 0 \end{cases} \quad (\text{A3})$$

The semidiscretized form of the energy Equation (11) then becomes

$$\frac{\partial T}{\partial t} = \bar{\alpha}(T)(\delta_x^2 + \delta_y^2)T - \beta(T)(v_x \delta_x + v_y \delta_y)T + Q(x, y, t). \quad (\text{A4})$$

For the time discretization, we choose the Crank-Nicolson method. After some manipulation, Equation (A4) becomes

$$\begin{aligned}\left[1 - \frac{\bar{\alpha}^{n+1} \Delta t}{2} (\delta_x^2 + \delta_y^2)\right] T^{n+1} &= \left[1 + \frac{\bar{\alpha}^n \Delta t}{2} (\delta_x^2 + \delta_y^2)\right] T^n - \\ &+ \left[\beta^n \Delta t (v_x \delta_x + v_y \delta_y)\right] T^n + \Delta t Q(x, y, t).\end{aligned}\quad (\text{A5})$$

Applying operator splitting, $\frac{1}{2}$ time step is taken and the x -direction is treated implicitly and y -direction is treated explicitly, followed by another $\frac{1}{2}$ time step where the y -direction is treated implicitly and the x -direction is treated explicitly. The finite-difference equations are

$$\left[1 - \frac{\bar{\alpha}^{n+1/2} \Delta t}{2} \delta_x^2\right] T^{n+1/2} = \quad (\text{A6})$$

$$\left[1 + \frac{\bar{\alpha}^n \Delta t}{2} \delta_y^2 - \beta^n \Delta t (v_y \delta_y)\right] T^n + \frac{\Delta t}{2} Q^n$$

$$\left[1 - \frac{\bar{\alpha}^{n+1} \Delta t}{2} \delta_y^2\right] T^{n+1} = \quad (\text{A7})$$

$$\left[1 + \frac{\bar{\alpha}^n \Delta t}{2} \delta_x^2 - \beta^n \Delta t (v_x \delta_x)\right] T^{n+1/2} + \frac{\Delta t}{2} Q^n.$$

The nonlinear term α^{n+1} results in a coupled set of nonlinear algebraic equations to solve at each time step. Instead, the problem was linearized by introducing

$$\bar{\alpha}(T^{n+1}) = \bar{\alpha}(T^n) + (T^n - T^{n-1}) \frac{\partial \bar{\alpha}}{\partial T}. \quad (\text{A8})$$

Expanding Equations (A6) and (A7) with the help of Equations (A1) through (A3) gives the final form of the difference equations to be solved

$$a_x T_{i-1,j}^{n+1/2} + b_x T_{i,j}^{n+1/2} + c_x T_{i+1,j}^{n+1/2} = d_y T_{i,j-1}^n + e_y T_{i,j}^n + f_y T_{i,j+1}^n + \frac{\Delta t}{2} Q_{i,j}^n \quad (A9)$$

$$a_y T_{i,j-1}^{n+1} + b_y T_{i,j}^{n+1} + c_y T_{i,j+1}^{n+1} = d_x T_{i-1,j}^{n+1/2} + e_x T_{i,j}^{n+1/2} + f_x T_{i+1,j}^{n+1/2} + \frac{\Delta t}{2} Q_{i,j}^n \quad (A10)$$

where

$$a_x = -\frac{\bar{\alpha}^{n+1} \Delta t}{2\Delta x^2} \quad a_y = -\frac{\bar{\alpha}^{n+1} \Delta t}{2\Delta y^2} \quad (A11)$$

$$b_x = \left(1 + \frac{\bar{\alpha}^{n+1} \Delta t}{\Delta x^2}\right) \quad b_y = \left(1 + \frac{\bar{\alpha}^{n+1} \Delta t}{\Delta y^2}\right) \quad (A12)$$

$$c_x = -\frac{\bar{\alpha}^{n+1} \Delta t}{2\Delta x^2} \quad c_y = -\frac{\bar{\alpha}^{n+1} \Delta t}{2\Delta y^2} \quad (A13)$$

$$d_x = \left\{ \begin{array}{l} \frac{\bar{\alpha}^n \Delta t}{2\Delta x^2} + \frac{\beta^n \Delta t}{\Delta x} v_x, v_x > 0 \\ \frac{\bar{\alpha}^n \Delta t}{2\Delta x^2}, v_x < 0 \end{array} \right. \quad (A14)$$

$$d_y = \left\{ \begin{array}{l} \frac{\bar{\alpha}^n \Delta t}{2\Delta y^2} + \frac{\beta^n \Delta t}{\Delta y} v_y, v_y > 0 \\ \frac{\bar{\alpha}^n \Delta t}{2\Delta y^2}, v_y < 0 \end{array} \right. \quad (A15)$$

$$e_x = \left\{ \begin{array}{l} 1 - \frac{\bar{\alpha}^n \Delta t}{2\Delta x^2} - \frac{\beta^n \Delta t}{\Delta x} v_x, v_x > 0 \\ 1 - \frac{\bar{\alpha}^n \Delta t}{2\Delta x^2} + \frac{\beta^n \Delta t}{\Delta x} v_x, v_x < 0 \end{array} \right. \quad (A16)$$

$$e_y = \left\{ \begin{array}{l} 1 - \frac{\bar{\alpha}^n \Delta t}{2\Delta y^2} - \frac{\beta^n \Delta t}{\Delta y} v_y, v_y > 0 \\ 1 - \frac{\bar{\alpha}^n \Delta t}{2\Delta y^2} + \frac{\beta^n \Delta t}{\Delta y} v_y, v_y < 0 \end{array} \right. \quad (A17)$$

$$f_x = \left\{ \begin{array}{l} \frac{\bar{\alpha}^n \Delta t}{2\Delta x^2}, v_x > 0 \\ \frac{\bar{\alpha}^n \Delta t}{2\Delta x^2} - \frac{\beta^n \Delta t}{\Delta x} v_x, v_x < 0 \end{array} \right. \quad (A18)$$

$$f_y = \left\{ \begin{array}{l} \frac{\bar{\alpha}^n \Delta t}{2\Delta y^2}, v_y > 0 \\ \frac{\bar{\alpha}^n \Delta t}{2\Delta y^2} - \frac{\beta^n \Delta t}{\Delta y} v_y, v_y < 0 \end{array} \right. \quad (A19)$$

BOUNDARY CONDITIONS

Difference equations for both Dirichlet and Neumann type boundary conditions will be derived here since both types of boundaries need to be simulated.

Dirichlet

Because wall temperatures on the boundary are specified, difference equations are derived from Equations (A9) and (A10) for one node in from the wall boundary

Left Wall

$$0 + b_x T_{2,j}^{n+1/2} + c_x T_{3,j}^{n+1/2} = d_y T_{2,j-1}^n + e_y T_{2,j}^n + f_y T_{2,j+1}^n + \frac{\Delta t}{2} Q_{2,j}^n + a_x T_1 \quad (A20)$$

Right Wall

$$a_x T_{m-1,j}^{n+1/2} + b_x T_{m,j}^{n+1/2} + 0 = d_y T_{m-1,j-1}^n + e_y T_{m-1,j}^n + f_y T_{m-1,j+1}^n + \frac{\Delta t}{2} Q_{m-1,j}^n + c_x T_3 \quad (A21)$$

Bottom

$$0 + b_y T_{i,2}^{n+1} + c_y T_{i,3}^{n+1} = d_x T_{i-1,2}^{n+1/2} + e_x T_{i,2}^{n+1/2} + f_x T_{i+1,2}^{n+1/2} + \frac{\Delta t}{2} Q_{i,2}^n + a_y T_2 \quad (A22)$$

Top

$$a_y T_{i,i-2}^{n+1} + b_y T_{i,i-1}^{n+1} + 0 = d_x T_{i-1,i-1}^{n+1/2} + e_x T_{i,i-1}^{n+1/2} + f_x T_{i+1,i-1}^{n+1/2} + \frac{\Delta t}{2} Q_{i,i-1}^n + c_y T_4 \quad (A23)$$

Neumann

Difference equations for the flux boundary condition are derived by introducing a fictitious grid one node beyond the boundary of each wall. The finite-difference equations for Equations (16) and (17) then are

$$\bar{k}_{1,j} \frac{T_{2,j} - T_{0,j}}{2\Delta x} = F_1 \quad \bar{k}_{m,j} \frac{T_{m-1,j} - T_{m+1,j}}{2\Delta x} = F_3 \quad (A24)$$

$$\bar{k}_{i,1} \frac{T_{i,2} - T_{i,0}}{2\Delta y} = F_2 \quad \bar{k}_{i,1} \frac{T_{i,i-1} - T_{i,i+1}}{2\Delta y} = F_4 \quad (A25)$$

Solving Equations (A24) and (A25) for the temperature at the fictitious grid point and substituting into Equations (A9) and (A10) the following equations are derived:

Left Wall

$$0 + b_x T_{1,j}^{n+1/2} + (a_x + c_x) T_{2,j}^{n+1/2} =$$

$$d_y T_{1,j-1}^n + e_y T_{1,j}^n + f_y T_{1,j+1}^n + \frac{\Delta t}{2} Q_{1,j}^n - \frac{\Delta t F_1}{\Delta x \rho C_{v,1}^{n+1}} \quad (\text{A26})$$

Right Wall

$$(a_x + c_x) T_{m-1,j}^{n+1/2} + b_x T_{m,j}^{n+1/2} + 0 =$$

$$d_y T_{m,j-1}^n + e_y T_{m,j}^n + f_y T_{m,j+1}^n + \frac{\Delta t}{2} Q_{m,j}^n - \frac{\Delta t F_3}{\Delta x \rho C_{v,m,j}^{n+1}} \quad (\text{A27})$$

Bottom

$$0 + b_y T_{i,1}^{n+1/2} + (a_y + c_y) T_{i,2}^{n+1/2} =$$

$$d_x T_{i-1,1}^n + e_x T_{i,1}^n + f_x T_{i+1,1}^n + \frac{\Delta t}{2} Q_{i,1}^n - \frac{\Delta t F_3}{\Delta y \rho C_{v,i,1}^{n+1}} \quad (\text{A28})$$

Top

$$(a_y + c_y) T_{i,j-1}^{n+1/2} + b_y T_{i,j}^{n+1/2} + 0 =$$

$$d_x T_{i-1,j}^n + e_x T_{i,j}^n + f_x T_{i+1,j}^n + \frac{\Delta t}{2} Q_{i,j}^n - \frac{\Delta t F_4}{\Delta y \rho C_{v,i,j}^{n+1}} \quad (\text{A29})$$

DIFFUSION-ADVECTION EQUATION

Similar sets of difference equations (A9 and A10) and associated boundary conditions can be derived for the diffusion-advection equation (12). The major difference occurs in dealing with the additional mass-action (5), and mass-balance equations (6). After completing a transport step, Equation (6) is solved to obtain new values for the concentration c_s . This is accomplished with

$$(c_s)_{i,j}^{n+1} = [1 - \lambda \Delta t] (c_s)_{i,j}^n - \frac{\rho_s}{\rho_l} [(c_l)_{i,j}^{n+1} - (c_l)_{i,j}^n] \quad (\text{A30})$$

Once the new values for the solid phase concentration are obtained, Equation (5) is solved to maintain equilibrium with the solid phase throughout the spatial domain provided $c_s > 0$.

REFERENCE

- ¹Peaceman, D. W., and H. H. Rachford. 1955. *J. Soc. Indus. Appl. Math.* 3:28-41.

DISTRIBUTION

<u>No. of Copies</u>		<u>No. of Copies</u>
OFFSITE		
12	<p>U.S. Department of Energy Office of Scientific and Technical Information</p> <p>Charles S. Abrams 1987 Virginia Idaho Falls, ID 83404</p> <p>Shirley Campbell-Grizzel U.S. Department of Energy EH-15, Trevion II 12800 Middlebrook Road Germantown, MD 20874</p> <p>George E. Schmauch Air Products & Chemicals, Inc. 7201 Hamilton Blvd. Allentown, PA 18195-1501</p> <p>James A. Gieseke Battelle Columbus Division 505 King Avenue Columbus, OH 43201-2693</p> <p>Kamal K. Bandyopadhyay Brookhaven National Laboratory Upton, NY 11973</p> <p>David O. Campbell 102 Windham Road Oak Ridge, TN 37830</p> <p>Fred N. Carlson 6965 North 5th West Idaho Falls, ID 83401</p> <p>Gary Powers Design Science, Inc. 163 Witherow Road Sewickley, PA 15143</p>	<p>Hans K. Fauske Fauske and Associates, Inc. 16W070 W. 83rd St. Burr Ridge, IL 60521</p> <p>Gregory R. Choppin Florida State University Department of Chemistry B-164 Tallahassee, FL 32306</p> <p>Melvin W. First Harvard University 295 Upland Avenue Newton Highlands, MA 02161</p> <p>Chester Grelecki Hazards Research Corporation 200 Valley Road, Suite 301 Mt. Arlington, NJ 07856</p> <p>Billy Hudson 202 Northridge Court Lindsborg, KA 67456</p> <p>Thomas S. Kress P.O. Box 2009 9108, MS-8088 Oak Ridge, TN 37831-8088</p>
		3
		<p>Los Alamos National Laboratory P.O. Box 1663 Los Alamos, NM 87545</p> <p>Steve F. Agnew Steve Eisenhower Thomas E. Larson</p> <p>Mujid S. Kazimi MIT/Dept of Nuclear Eng. 77 Massachusetts Avenue Room 24-102 Cambridge, MA 02139</p>

<u>No. of Copies</u>		<u>No. of Copies</u>	
	Louis Kovach Nuclear Consulting Serices, Inc. P.O. Box 29151 Columbus, OH 43229-0151		Alex Stone 1105 W. 10th Ave., #236 Kennewick, WA 99336-6018
2	Oak Ridge National Laboratory P.O. Box 2008 Oak Ridge, TN 37831-6385 Emory D. Collins, MS-6385 Charles W. Forsberg, MS-6495	6	U.S. Department of Energy EM-36, Trevion II 12800 Middlebrook Road Germantown, MD 20874 James V. Antizzo Charles O'Dell (5)
	Arlin K. Postma 3640 Ballard Road Dallis, OR 97338		Thomas C. Temple U.S. Department of Energy Savannah River Operations Office P.O. Box A Aiken, SC 29808
	William R. Prindle 1556 Crestline Drive Santa Barbara, CA 93105		Bruce R. Kowalski University of Washington Center for Process Analytical Chemistry Chemistry Department BG-10 Seattle, WA 98195
	Andrew S. Veletsos Rice University 5211 Paisley Houston, TX 77096		Joseph S. Byrd University of South Carolina Department of Electrical and Computer Engineering Swearingen Engineering Center Columbia, SC 29208
2	Sandia National Laboratories P.O. Box 5800 Albuquerque, NM 87185 Scott E. Slezak, MS-0741 Dana Powers, MS-0744		Frank L. Parker Vanderbilt University P.O. Box 1596, Station B Nashville, TN 37235
	Alfred Schneider 5005 Hidden Branches Drive Dunwoody, GA 30338		Donald T. Oakley Waste Policy Institute 555 Quince Orchard Road, Ste 600 Gaithersburg, MD 20878-1437
3	Ray S. Daniels Science Applications International Corporation 20300 Century Blvd., Suite 200-B Germantown, MD 20874		
	Michael T. Gordon State of Washington Department of Ecology P. O. Box 47600 Olympia, WA 98504-7600		

No. of
CopiesNo. of
Copies**ONSITE**

12 **U.S. Department of Energy
Richland Operations Office**
R. F. Christensen, S7-54 (4)
R. E. Gerton, S7-54 (4)
A. G. Krasopoulos, A4-81
Public Reading Room, H2-53
RL Docket File, H5-36 (2)

37 **Westinghouse Hanford Company**
H. Babad, S7-30
J. B. Billetdeaux, S7-16
D. C. Board, S1-57
G. L. Borsheim, H5-27
R. J. Cash, S7-15 (2)
M. D. Crippen, L5-31
D. R. Dickinson, L5-31
G. T. Dukelow, S7-15
J. M. Grigsby, H4-62
M. E. Huda, R3-08
M. N. Islam, R3-08
D. W. Jeppson, L5-31
N. W. Kirch, R2-11
C. A. Kuhlman, B3-30
M. Kummerer, H4-62
J. M. McLaren, H0-34
J. E. Meacham, S7-15
N. J. Milliken, H4-63
S. R. Moreno, B3-06
M. A. Payne, S7-14
F. R. Reich, L5-55
C. P. Schroeder, L7-06
B. C. Simpson, R2-12
H. Toffer, H0-38
W. T. Watson, H0-38
W. D. Winkelman, L5-55
D. D. Wodrich, S7-84
W. F. Zuroff, S7-12
Central Files, L8-04

Document Processing and
Distribution, L8-15 (2)
EDMC, H6-08
Information Release
Administration, R1-05 (3)
TFIC, R1-20

28 **Pacific Northwest Laboratory**
R. M. Bean, P8-08
J. W. Brothers, K5-22
S. A. Bryan, K5-82
L. L. Eyler, K7-15
L. L. Fassbender, K8-18
A. R. Felmy, K6-82
S. C. Goheen, P8-08
B. M. Johnson, K1-78
M. A. Lilga, P8-38
B. P. McGrail, K2-38 (5)
A. F. Noonan, B1-40
A. W. Prichard, K8-34
D. Rai, K6-82
R. D. Scheele, P7-25
G. F. Schiefelbein, P8-38 (2)
C. W. Stewart, K7-15
D. M. Strachan, K2-44
Publishing Coordination
Technical Report Files, K1-11 (5)